THE GERONTOLOGICAL SOCIETY OF AMERICA®

Journals of Gerontology: Biological Sciences
cite as: *J Gerontol A Biol Sci Med Sci*, 2021, Vol. 76, No. 7, 1169–1178
doi:10.1093/gerona/glab075
Advance Access publication March 12, 2021

OXFORD

Original Article

Impaired Cognitive Flexibility Induced by Chronic Cerebral Hypoperfusion in the 5XFAD Transgenic Mouse Model of Mixed Dementia

Min-Soo Kim, MS,[1,2] Jihye Bang, PhD,[1,2] Bu-Yeo Kim, PhD,[1] and Won Kyung Jeon, PhD[1,2,*]

[1]Herbal Medicine Research Division, Korea Institute of Oriental Medicine, Daejeon, South Korea. [2]Convergence Research Center for Diagnosis, Treatment and Care System of Dementia, Korea Institute of Science and Technology, Seoul, South Korea.

*Address correspondence to: Won Kyung Jeon, PhD, Korea Institute of Oriental Medicine, Daejeon 34054, South Korea. E-mail: wkjeon@kiom.re.kr

Received: September 6, 2020; Editorial Decision Date: February 14, 2021

Decision Editor: Rozalyn M. Anderson, PhD, FGSA

Abstract

Cerebrovascular lesions are widely prevalent in patients with Alzheimer's disease (AD), but their relationship to the pathophysiology of AD remains poorly understood. An improved understanding of the interaction of cerebrovascular damage with AD is crucial for the development of therapeutic approaches. Herein, we investigated the effects of chronic cerebral hypoperfusion (CCH) in a 5XFAD transgenic (Tg) mouse model of AD. We established CCH conditions in both Tg and non-Tg mice by inducing unilateral common carotid artery occlusion (UCCAO). Cognitive performance in mice was evaluated, and their brain tissue was examined for amyloid-beta (Aβ) pathology to elucidate possible mechanisms. We found that UCCAO-operated Tg mice showed impaired cognitive flexibility in the reversal phase of the hidden-platform water maze task compared to sham-operated Tg mice. Interestingly, UCCAO-operated Tg mice used fewer spatial cognitive strategies than sham-operated Tg mice during reversal learning. These cognitive deficits were accompanied by increased Aβ plaque burden and Aβ42 levels in the hippocampus and prefrontal cortex, 2 regions that play essential roles in the regulation of cognitive flexibility. Furthermore, changes in cognitive flexibility are strongly correlated with the expression levels of enzymes related to Aβ clearance, such as neprilysin and insulin-degrading enzymes. These findings suggest that, in 5XFAD mice, impaired cognitive flexibility is related to CCH, and that Aβ clearance might be involved in this process.

Keywords: Alzheimer's disease, Amyloid-beta, Reversal learning, Unilateral common carotid artery occlusion

For the past 20 years, many studies have been conducted to develop a cure for Alzheimer's disease (AD), a progressive neurodegenerative disorder affecting an increasing number of people. However, treatments effective in animal studies have largely failed to translate to humans; thus, since the early 2000s, no new drugs have been approved for treating AD (1). These successive failures have led researchers to reconsider the causes of AD.

In general, dementia is defined as a condition associated with multifaceted progressive cognitive deficits and can be subdivided into AD and non-AD, the latter group including vascular dementia (VaD), frontotemporal dementias, and Lewy body dementia (2). However, it is difficult to identify distinct subtypes of dementia, because multiple dementias often coexist in the same patient (3), a situation often referred to as mixed dementia (MD). Among MDs, VaD in combination with AD is the most common form, accounting for approximately 50% of all dementia patients (4,5). Vascular dementia is mainly characterized by a heterogeneous pathology involving white matter lesions and neurological dysfunction (6,7), and many clinical studies have suggested that cerebral hypoperfusion can lead to VaD and/or MD progression (8,9). In fact, oxidative stress, inflammatory responses, and amyloid-beta (Aβ) accumulation, which are also common to the pathology of AD, have been previously reported to be associated with chronic cerebral hypoperfusion (CCH) (10–12). Moreover, CCH is present at "early" stages of AD. Further, alterations in cerebral blood flow (CBF) have been detected by arterial spin-labeling magnetic resonance imaging before the onset of explicit AD symptoms (13,14), which suggest the potential of CCH as a biomarker of AD. Therefore, since cerebrovascular damage can

trigger the progression of dementia (15,16), it is important to consider vascular factors in AD research.

Owing to the limitations of using transgenic (Tg) mice targeting Aβ as an important diagnostic hallmark of AD, there is a growing need for developing newer animal AD models capable of reflecting the pathophysiology of VaD (9). A previous study showed that the J20 strain, a mouse model of AD overexpressing human amyloid precursor protein (APP) with the Swedish and Indiana mutations, in combination with CCH, one of the most common causes of VaD, exhibited impaired learning ability compared to AD mice (17). Another study demonstrated that the CCH + APP23 AD mice (expressing human vasculotropic Swedish mutant APP) showed aggravated cognitive dysfunction in an 8-arm radial maze with Aβ accumulation compared to APP23 alone (18). Furthermore, increased Aβ40 deposition was reported in the cerebral cortex of CCH model of APP23 AD mice (19), while spatial learning ability became more impaired after CCH surgery in Tg 2576 mice (a mouse model overexpressing human APP_{695} with the Swedish mutation) than in the Tg 2576 mice without CCH (20). However, a systematic evaluation of learning and memory from simple to higher-order cognition in MD animal models has not been fully undertaken. Moreover, the molecular links between AD and VaD have not been sufficiently clarified to develop successful drug treatments for dementia.

Thus, we systematically investigated the effect of CCH on learning and memory in an AD mouse model. The Y-maze and water maze tasks were performed in succession to test for working memory, spatial learning, and spatial memory. We also investigated reversal learning and memory to test cognitive flexibility, which is a central feature of higher-order cognition (21). Alterations in Aβ40, Aβ42, and plaque load in the brain were measured by immunofluorescence staining and sandwich enzyme-linked immunosorbent assay (ELISA). Further, we examined the expression level of proteins related to Aβ production and clearance using western blots to explore the molecular evidence linking CCH with AD. Finally, we used microarray analysis to briefly analyze gene expression patterns and pathways to investigate the molecular differences between groups.

Method

Animals

Three-month-old male 5XFAD Tg mice (n = 20) harboring both mutant human APP (K670N, M671L, I716V, V717I) and presenilin 1 (M146L * L286V), as well as their non-Tg control littermates (n = 16), were used in the present study. It has been reported that by age 3 months, Aβ plaques already start to appear in this mouse model (22); thus, we adopted this age to investigate the effects of CCH on Tg mice. 5XFAD Tg mice were purchased from Jackson Laboratories (Bar Harbor, ME) and maintained by crossing hemizygous Tg mice with non-Tg B6/SJL breeders (Jackson Laboratories). All newborn pups were screened for transgene expression by polymerase chain reaction analysis, as described in the Jackson Laboratory protocol. Mice were housed in groups of 2–4 per cage under standard laboratory conditions (12-hour light/dark cycle; lights on at 8:00–20:00, temperature: 23 ± 2 °C, and humidity: 50% ± 10%) with ad libitum access to food and water.

Experimental Design

Mice were randomly divided into groups and subjected to unilateral common carotid artery occlusion (UCCAO) for the induction of CCH, or sham surgery. Four groups were defined in this study: (i) non-Tg + SHAM (n = 8); (ii) non-Tg + UCCAO (n = 8); (iii) Tg + SHAM (n = 10); and (iv) Tg + UCCAO (n = 10). In order to generate CCH, right UCCAO surgery was performed according to our previous report (23). The detailed surgical procedure and a schematic design of the present study are shown in the Supplementary Figure 1A.

Open Field Test

The animals were placed in the middle of a square arena (40 × 40 × 40 cm) and allowed to explore freely for 10 minutes. Locomotor behavior was continuously recorded by a camera, and the total distance moved and time spent in the center (24 × 24 cm) were scored with video tracking software (HVS Image, Bicester, UK). The arena was cleaned with a 70% ethanol solution and a dry paper towel after each trial.

Y-Maze Task

The Y-maze task can be used to evaluate short-term working memory, as previously described (24). The animals were placed in the junction of 3 identical arms (40 × 10 × 15 cm with the 120° angle between arms) and given free access to the arms for an 8-minute session. The entry of mice into each arm was video-recorded, and the sequence and number of arms entered were analyzed. Spontaneous alternation was calculated according to the following equation:

$$\text{Spontaneous alternation}\,(\%) = \frac{\text{Number of alternations}}{\text{Total arm entries} - 2} \times 100$$

Water Maze Task

Long-term spatial memory was assessed using the water maze task, as previously described, but with minor modifications (25). The experimental procedures consisted of 3 phases: the acquisition learning phase, reversal learning phase, and cued trials.

The acquisition learning phase consisted of 4 trials daily (10-minute intertrial interval, maximum trial duration of 60 seconds) for 7 days (Days 1–7). On training Days 3 and 7, probe tests (without the platform) were conducted. In the reversal learning phase, the platform was placed in the opposite quadrant for 3 days (Days 8–10). On training Day 10, the probe test was also conducted. On Day 11, the cued trials were conducted. In these trials, the visible platform, marked with a salient black tape, was raised 2 cm above the water surface and moved to different positions across trials (4 trials/d). Detailed methods are provided in the Supplementary Material, and a schematic design of the water maze protocol is shown in Supplementary Figure 1B.

Analysis of Search Strategies

The swimming pattern of each mouse during the water maze task was classified into 10 search strategies according to the criterion described previously (26,27). Supplementary Figure 2 shows the classification of search strategies and representative swim paths for mice using 10 different strategies. Detailed methods are provided in the Supplementary Material.

Immunofluorescence Staining

To investigate Aβ plaque accumulation, immunofluorescence staining was conducted as previously described (28). Serial sections from the prefrontal cortex (PFC; bregma, 1.94–1.42 mm) to the hippocampus

(bregma, −1.70 to −2.18 mm) were used for immunofluorescent staining. Three sections per animal were blocked with 5% normal goat serum (Vector Laboratories) and then immersed in anti-mouse 6E10 primary antibody (BioLegend) overnight at 4 °C. Sections were immersed in Alexa Fluor conjugated secondary antibody (Invitrogen) for 90 minutes, and incubated in 4′-6-diamidino-2-phenylindole solution (Sigma-Aldrich) for 10 minutes to stain the cellular nuclei. Stained sections were imaged using a fluorescence microscope (Olympus, Japan), and Aβ plaque load in the hippocampal subregions (CA1: cornu ammonis 1 and DG: dentate gyrus) and PFC (PL: prelimbic cortex and IL: infralimbic cortex) was quantified using Image J software (NIH). For Aβ plaque load analysis, the number of 6E10-positive pixels was divided by the number of whole pixels in each image and, according to previous reports (18,29), the data are reported as the percentage area occupied by the 6E10-positive signal. To apply the same selection criteria to all cuts, a template was created from a region of interest in the hippocampus and PFC and applied on each sample.

Sandwich ELISA

Aβ peptide levels were measured using commercially available mouse Aβ40 and Aβ42 ELISA kits (Invitrogen). All assays, including sample preparation, were conducted following the manufacturer's instructions. The absorbance of the ELISA well plate was read at 450 nm using a microplate reader (BioTek).

Western Blot

Western blot analysis was performed as previously described (30). Tissues were homogenized on ice in radio-immunoprecipitation assay (RIPA) buffer, and equivalent amounts of samples were fractionated by sodium dodecyl sulfate (SDS)–gel electrophoresis, transferred onto polyvinylidene difluoride membranes, and blocked with 5% nonfat milk in phosphate-buffered saline containing Tween-20. The membrane was incubated in primary antibodies overnight at 4 °C. Protein bands were imaged using an imaging system (ProteinSimple), and quantified using the Image Gauge program (Fujifilm, Japan). Detailed information of the primary antibodies use is presented in Supplementary Table 1.

Microarray Analyses

RNA isolation and microarray analyses were performed as previously described, with minor modifications. Detailed methodology is provided in the Supplementary Material.

Statistical Analysis

All data are expressed as the mean ± *SEM*. The data shown are the average of 2 independent replicate experiments. The homogeneity of variances of each data set was analyzed using the Levene's test. The latencies of the water maze task were analyzed using a repeated measures 3-way analysis of variance (ANOVA) with genotype, CCH, and day as main effects, along with the interactions. For analysis of search strategies, a 2-way ANOVA was used to test whether group, strategy, and their interaction were significant. For other comparisons, a 1-way or 2-way ANOVA was performed followed by least significant difference or Tamhane post-hoc test. A p-value <.05 was considered statistically significant. Correlation analysis was performed using the Pearson correlation coefficient, and R^2 values are included in the graphs. All statistical analyses were performed using SPSS software (IBM Corp.). Detailed F and p values for each ANOVA analysis are presented in Supplementary Table 2.

Results

Chronic Cerebral Hypoperfusion Exacerbates Impairment of Reversal Learning and Memory in 5XFAD Mice

We first measured the locomotor activity of mice using an open field test to assess the effect of CCH on general motor behavior and anxiety level. During the 10-minute test, there were no significant differences in the total distance traveled between groups (Supplementary Figure 3A), suggesting that CCH did not induce any locomotor disturbance. In addition, the amount of time spent in the center zone was comparable between groups (Supplementary Figure 3B), suggesting that CCH did not affect anxiety level.

Next, short-term working memory was assessed using the Y-maze task, a widely accepted tool for evaluating the ability to temporarily hold and manipulate information (31). There were no significant differences in the total number of arm entries (Supplementary Figure 4B), indicating similar explorative behavior between groups. The spontaneous alternation ratio of the other groups (non-Tg + UCCAO and Tg + SHAM) was significantly lower than that of the non-Tg + SHAM group, but there was no significant difference between Tg + SHAM or non-Tg + UCCAO and Tg + UCCAO (Supplementary Figure 4A).

To evaluate long-term spatial learning and memory, a water maze task was used. Initially, no significant differences in swimming speed were observed between groups during the learning phase (Supplementary Figure 5), which again suggests that none of the mice had a motor impairment. Figure 1A shows the mice swim latency during training sessions in the water maze. In the acquisition phase, 3-way repeated measures ANOVA revealed a significant main effect of genotype ($F_{(1,224)} = 123.781$, $p < .001$) and day ($F_{(6,224)} = 23.002$, $p < .001$), though the main effect of CCH ($F_{(1,224)} = 2.768$, $p = .098$) was not statistically significant. We also observed interactions between Genotype × CCH ($F_{(1,224)} = 5.388$, $p = .021$) and Genotype × Day ($F_{(6,224)} = 7.188$, $p < .001$), but there were no significant CCH × Day interactions ($F_{(6,224)} = 0.633$, $p = .704$). Post-hoc tests showed that Tg + SHAM mice performed worse than non-Tg + SHAM mice during acquisition learning ($p < .001$). Additionally, UCCAO-exposed non-Tg groups were significantly better in finding the escape platform than the Tg group ($p < .001$). However, we did not observe synergistic learning impairments in Tg + UCCAO compared to Tg + SHAM mice. Figure 1B and C show the data obtained from probe tests for the assessment of spatial retention memory. The 2-way ANOVA revealed a significant main effect of genotype ($F_{(1,32)} = 6.030$, $p = .020$ for the first, and $F_{(1,32)} = 7.775$, $p = .009$ for the second probe test), but there was no significant main effect of CCH or Genotype × CCH interactions, in the time to the target quadrant (Figure 1B). Post-hoc analysis showed that Tg + UCCAO mice spent less time swimming in the target quadrant than non-Tg + UCCAO mice did ($p = .030$ for the first, and $p = .018$ for the second probe test). In terms of the number of platform position crossings (Figure 1C), Tg + SHAM and Tg + UCCAO mice exhibited lesser number of platform crossings than the non-Tg + UCCAO mice during the second probe test ($p < .001$). Consistent with the acquisition learning results, there was no difference between Tg + SHAM and Tg + UCCAO mice in the probe tests.

In line with a previous study (25), 3 additional days of reversal learning were conducted to evaluate the cognitive flexibility of mice after the acquisition learning phase. Three-way repeated measures ANOVA revealed a significant main effect of genotype ($F_{(1,96)} = 73.106$, $p < .001$), CCH ($F_{(1,96)} = 11.950$, $p < .001$), and day

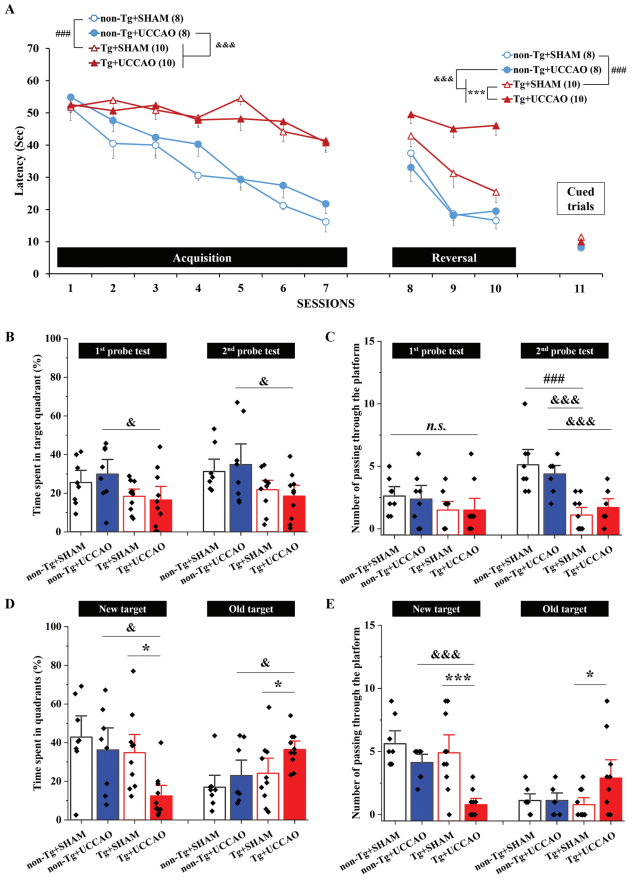

Figure 1. Spatial learning and memory in 5XFAD mice with unilateral common carotid artery occlusion (UCCAO). Spatial learning was measured using the water maze protocol consisting of acquisition and reversal phases, followed by cued platform trials. Reference memory of mice was examined on Day 3 (first probe test), Day 7 (second probe test), and Day 10 (reversal probe test). (**A**) Learning curves of the acquisition (7 d) and reversal phases (3 d) were described in terms of latency (s) to find the hidden platform. Latency in the cued platform trials was also described at the last (11th) day. (**B**) Time spent in the target quadrant and (**C**) crossing times at platform position during the probe trial on Day 3 (first) and 7 (second). (**D**) Time spent in the target quadrant and (**E**) crossing times at platform position during the reversal probe test on Day 10. Numbers in parentheses describe the number of samples. Data are presented as the mean ± *SEM*. $^{\#\#\#}p < .001$ compared with non-Tg + SHAM group; $^{\&}p < .05$ and $^{\&\&\&}p < .001$ compared with non-Tg + UCCAO group; $^{*}p < .05$ and $^{***}p < .001$ compared with Tg + SHAM group. *n.s.* = nonsignificant.

($F_{(2,96)}$ = 21.629, p < .001). The interaction between genotype and CCH ($F_{(1,96)}$ = 14.483, p < .001) was significant, though Genotype × Day ($F_{(2,96)}$ = 1.993, p = .142) and CCH × Day interactions ($F_{(2,96)}$ = 2.676, p = .074) were not statistically significant (Figure 1A). Post-hoc testing showed that Tg + SHAM mice performed worse than non-Tg + SHAM mice during reversal learning (p < .001). In addition, Tg + SHAM and Tg + UCCAO groups displayed impaired reversal learning abilities compared to non-Tg + UCCAO mice (p < .001). Interestingly, the Tg + UCCAO mice performed significantly worse than the Tg + SHAM mice (p < .001), indicating that cognitive flexibility was affected by CCH in 5XFAD mice. Figure 1D and E show the data obtained from probe tests for the assessment of reversal memory. The 2-way ANOVA revealed a significant main effect of genotype ($F_{(1,32)}$ = 6.587, p = .015 for new target, and $F_{(1,32)}$ = 5.288, p = .028 for old target quadrant) and CCH ($F_{(1,32)}$ = 5.468, p = .026 for new target, and $F_{(1,32)}$ = 4.157, p = .050 for old target), but there were no significant Genotype × CCH interactions in the time taken to reach the target quadrant (Figure 1D). Post-hoc analysis showed that Tg + UCCAO mice spent more time in the acquisition target quadrant than in the new target quadrant, which changed in the reversal learning phase, relative to the other groups (Figure 1D). In addition, Tg + UCCAO mice displayed a lower number of new platform location entries than the other groups (Figure 1E; p < .001).

On the last day (Day 11), mice were tested in cued trials in which the platform was changed to a marked visible platform. No significant differences were found between groups in the latency to find the salient black platform (Figure 1A), indicating that none of the mice had visual impairments. Together, these results suggest that CCH specifically induces reversal memory deficits in 5XFAD mice in the absence of visual impairment.

Chronic Cerebral Hypoperfusion Results in Decreased Use of Spatial Search Strategies in 5XFAD Mice During Reversal Learning

We further analyzed the search strategies for the last day of acquisition (on Day 7) and reversal learning phase (on Day 10), respectively. As shown in Figure 2A, there was a significant main effect of strategy ($F_{(8,288)}$ = 4.729, p < .001) as well as Strategy × Group interactions ($F_{(24,288)}$ = 3.213, p = .001) in acquisition learning. Post-hoc analysis showed that the non-Tg + SHAM group used a significantly more "spatial direct" strategy than the other groups (p < .001). In addition, Tg + SHAM mice and Tg + UCCAO mice showed less use of "focal correct" strategy than non-Tg + UCCAO mice (p = .030). However, we did not find a significant difference when comparing Tg + UCCAO mice with Tg + SHAM group mice in acquisition learning.

By analyzing the mice's strategies during reversal learning, we observed a significant main effect of strategy ($F_{(9,230)}$ = 10.595, p < .001) with Strategy × Group interactions ($F_{(27,320)}$ = 3.227, p < .001; Figure 2B). Post-hoc analysis showed that the Tg + UCCAO group used significantly less "spatial direct" and "spatial indirect" strategies compared to Tg + SHAM mice (p = .031 for spatial direct; p = .047 for spatial indirect). On the other hand, Tg + UCCAO mice showed a significant preference for "chaining" and "peripheral looping" strategies compared to non-Tg + UCCAO or Tg + SHAM mice (p = .030 for chaining; p = .026 for peripheral looping). Especially noteworthy is the result that Tg + UCCAO mice used significantly more "perseveration" than Tg + SHAM mice (p = .015), indicating that these group had difficulties to acquire newly updated information. Consistent with these results, classifying 10 strategies into one of the 4 main categories (spatial, nonspatial, repetitive, and perseveration) also resulted in a significant main effect of strategy ($F_{(3,288)}$ = 33.120, p < .001) as well as Strategy × Group interactions ($F_{(9,288)}$ = 10.533, p < .001; Figure 2C). Collectively, these results suggest that CCH affects the deployment of spatial cognitive strategies in 5XFAD mice during reversal learning.

Chronic Cerebral Hypoperfusion Increases Aβ Plaque and Aβ42 Levels in the Hippocampus and PFC of 5XFAD Mice

Aβ plaque burden in the mouse brain, one of the major hallmarks of AD, was measured using immunofluorescence staining to investigate whether Aβ pathology is involved in these reversal learning deficits. We focused on the analysis of the hippocampus and PFC because reversal learning and behavioral flexibility mainly depend on functional connections between these 2 regions (26,32). Comparison of

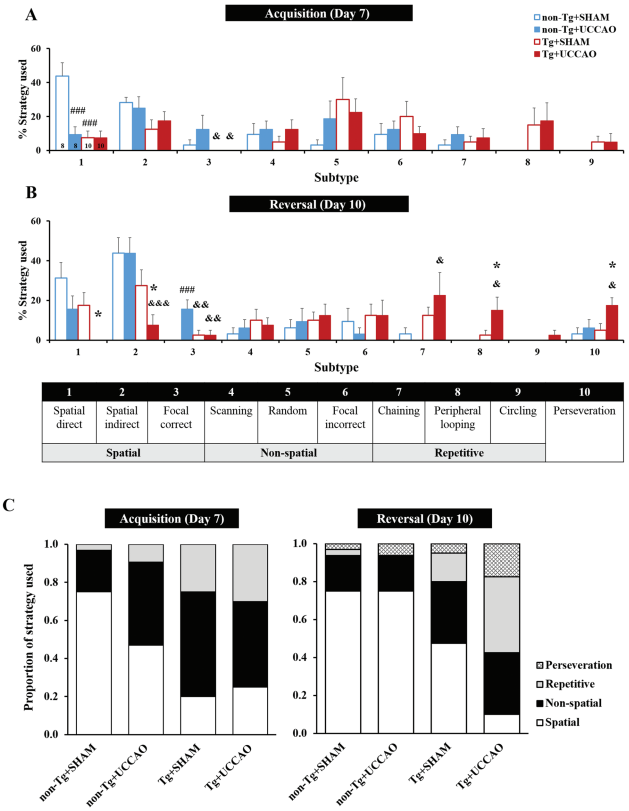

Figure 2. Different spatial search strategy in 5XFAD mice with unilateral common carotid artery occlusion (UCCAO). The use of search strategies during the last day of the (**A**) acquisition phase (on Day 7) and (**B**) reversal phase (on Day 10) was analyzed. The numbers in the x-axis refer to the different subcategories of search strategies as listed below and in Supplementary Figure 2, which are: (1) spatial direct, (2) spatial indirect, (3) focal correct, (4) scanning, (5) random, (6) focal incorrect, (7) chaining, (8) peripheral looping, (9) circling, and (10) perseveration. Subtypes 1–3 are grouped as spatial, 4–6 as nonspatial, and 7–9 as repetitive. The 10th strategy ("perseveration") is only applicable to the reversal phase. (**C**) Proportional use of major categories of search strategies during the last day of acquisition (on Day 7) and reversal phase (on Day 10). Data are presented as the mean ± *SEM*. $^{###}p < .001$ compared with non-Tg + SHAM group; $^{\&}p < .05$, $^{\&\&}p < .01$, and $^{\&\&\&}p < .001$ compared with non-Tg + UCCAO group; $^{*}p < .05$ compared with Tg + SHAM group.

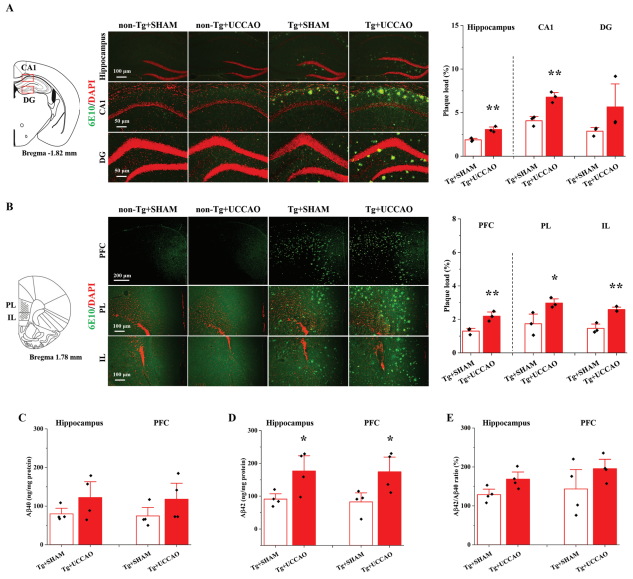

Figure 3. Aβ plaques and levels of Aβ40 and Aβ42 in the hippocampus and prefrontal cortex (PFC) of 5XFAD mice with unilateral common carotid artery occlusion (UCCAO). (**A, B**) The Aβ plaques were stained with anti-6E10 antibody (green) and the nuclei were counterstained with 4′,6-diamidino-2-phenylindole (red). *N* = 3 per group. (A) Left: Schematic illustration of the regions of interest depicted in the cornu ammonis 1 (CA1) and dentate gyrus (DG) areas of the hippocampus. The hippocampus and its subregions (CA1 and DG) were analyzed at −1.70 to −2.18 mm from bregma. Middle: Representative images of Aβ plaques in the hippocampus and its subregions. Right: Quantitative analysis of Aβ plaque burden (%). (B) Left: Schematic illustration of the regions of interest depicted in the prelimbic (PL) and infralimbic (IL) subdivisions of the PFC. The PFC and its subregions (PL and IL) were analyzed at 1.94–1.42 mm from bregma. Middle: Representative images of Aβ plaques in the PFC and its subregions. Right: Quantitative analysis of Aβ plaque burden (%). (**C–E**) Quantification of Aβ40 (C) and Aβ42 (D) in brain lysate analyses by sandwich enzyme-linked immunosorbent assay. Values are expressed as nanograms of Aβ40 or Aβ42 per milligram of total protein. (E) The ratio of Aβ42 to Aβ40 (%). *N* = 4 per group. Data are presented as the mean ± *SEM*. $^{*}p < .05$ and $^{**}p < .01$ compared with Tg + SHAM group.

the ipsilateral and contralateral sides did not show significant differences in Aβ plaque load in Tg + UCCAO mice (Supplementary Figure 6); thus, we selected each ipsilateral region and compared the groups for subsequent analyses. An ANOVA of the levels of hippocampal plaque load showed significant main effects of genotype (whole: $F_{(1,8)} = 288.255$, $p < .001$; CA1: $F_{(1,8)} = 442.487$, $p < .001$; DG: $F_{(1,8)} = 19.724$, $p = .002$), CCH (whole: $F_{(1,8)} = 21.238$, $p = .002$; CA1: $F_{(1,8)} = 29.120$, $p = .001$) as well as Genotype × CCH interactions (whole: $F_{(1,8)} = 20.923$, $p = .002$; CA1: $F_{(1,8)} = 33.776$, $p < .001$). Post-hoc testing showed that Tg + UCCAO mice exhibited remarkable increases in Aβ plaque load relative to Tg + SHAM mice in the whole hippocampus ($p = .006$) and CA1 (Figure 3A, $p = .005$). In the analysis of PFC and its subregions (PL and IL), we also observed significant main effects of genotype (whole: $F_{(1,8)} = 208.149$, $p < .001$; PL: $F_{(1,8)} = 96.824$, $p < .001$; IL: $F_{(1,8)} = 339.786$, $p < .001$), CCH (whole: $F_{(1,8)} = 22.681$, $p = .001$; PL: $F_{(1,8)} = 8.524$, $p = .019$; IL: $F_{(1,8)} = 33.849$, $p < .001$), and Genotype × CCH interactions (whole: $F_{(1,8)} = 12.528$, $p = .008$; PL: $F_{(1,8)} = 7.786$, $p = .024$; IL: $F_{(1,8)} = 31.268$, $p = .001$). Similar to the hippocampus, more Aβ plaque accumulation was observed in Tg + UCCAO mice than in the Tg + SHAM group mice in the PFC region (Figure 3B, $p = .010$ for PFC; $p = .044$ for PL; $p = .005$ for IL).

As Aβ plaques were increased in Tg + UCCAO mice, Aβ peptides including Aβ40 and Aβ42, which are the starting points for plaque aggregation, were measured. An ANOVA of Aβ40 levels revealed a significant main effect of genotype (hippocampus: $F_{(1,12)} = 37.417$, $p < .001$; PFC: $F_{(1,12)} = 28.192$, $p < .001$), but there was no significant main effect of CCH and Genotype × CCH interactions. Post-hoc testing showed that the Aβ40 level in Tg + UCCAO group was not significantly different than that in Tg + SHAM group. In contrast, in Aβ42 levels, we observed a significant main effect of genotype (hippocampus: $F_{(1,12)} = 58.648$, $p < .001$; PFC: $F_{(1,12)} = 36.351$, $p = .001$), CCH (hippocampus: $F_{(1,12)} = 6.863$, $p = .022$; PFC: $F_{(1,12)} = 4.729$, $p = .050$) as well as Genotype × CCH interactions (hippocampus: $F_{(1,12)} = 6.879$, $p = .022$; PFC: $F_{(1,12)} = 4.822$, $p = .048$). Post-hoc analysis revealed a significant increase in Aβ42 levels between Tg + UCCAO mice and Tg + SHAM mice in both regions (Figure 3D; $p = .040$). These results indicate more obvious changes in Aβ42 levels than in Aβ40 levels. Similar trends in the ratio of Aβ42 to Aβ40 in both the hippocampus and PFC are shown in Figure 3E.

Taken together, these results suggest that CCH exacerbates Aβ accumulation in the hippocampus and PFC of 5XFAD mice, but not in their non-Tg littermates.

Chronic Cerebral Hypoperfusion Reduces Expression Levels of Proteins Associated With Aβ Clearance in 5XFAD Mice

To further examine the underlying mechanisms regarding the increased Aβ plaque and Aβ42 in the hippocampus and PFC of Tg + UCCAO mice, we next investigated the expression levels of several proteins capable of Aβ clearance and production. First, we analyzed the expression of 2 proteins related to Aβ clearance, neprilysin and insulin-degrading enzyme (IDE). With respect to neprilysin levels, there was a significant main effect of genotype (hippocampus: $F_{(1,12)} = 51.809$, $p < .001$; PFC: $F_{(1,12)} = 10.425$, $p = .007$). Post-hoc testing showed that Tg + UCCAO mice showed significantly lower neprilysin levels than Tg + SHAM mice in both regions (Figure 4A; $p = .027$ for hippocampus; $p = .033$ for PFC). As for IDE levels, a significant main effect of genotype ($F_{(1,12)} = 6.619$, $p = .024$) and CCH ($F_{(1,12)} = 9.755$, $p = .009$) was detected in the PFC. In concordance with the results of neprilysin, IDE expression was decreased in Tg + UCCAO mice compared with Tg + SHAM mice in both regions (Figure 4B; $p = .004$ for hippocampus; $p = .010$ for PFC).

Second, we investigated the expression levels of proteins related to Aβ production, such as APP, β-site APP cleavage enzyme (BACE), disintegrin, and metalloproteinase 10 (a disintegrin and metalloproteinase 10 [ADAM10]; Figure 4C). It has been widely reported that Aβ is generated from APP by the action of BACE, whereas Aβ formation is prevented by ADAM10 (33). Considering ADAM10 levels, a significant main effect of genotype ($F_{(1,12)} = 14.957$, $p = .002$) was detected in the hippocampus. Post-hoc testing showed that Tg + UCCAO exhibited a remarkable decrease in ADAM10 levels relative to Tg + SHAM mice in the hippocampus (Figure 4D; $p = .042$), but not in the PFC. For the BACE levels, only a main effect of genotype ($F_{(1,12)} = 7.669$, $p = .017$) in the hippocampus was detected by ANOVA. Despite increase in BACE expression in the hippocampus of Tg + UCCAO mice, it was not significantly different from that of Tg + SHAM (Figure 4E; $p > .05$). As for APP expression levels, no difference between groups was observed in either the hippocampus or the PFC (Figure 4F). Collectively, these findings imply that CCH increased Aβ accumulation in 5XFAD mice, potentially by reducing the levels of enzymes involved in Aβ clearance.

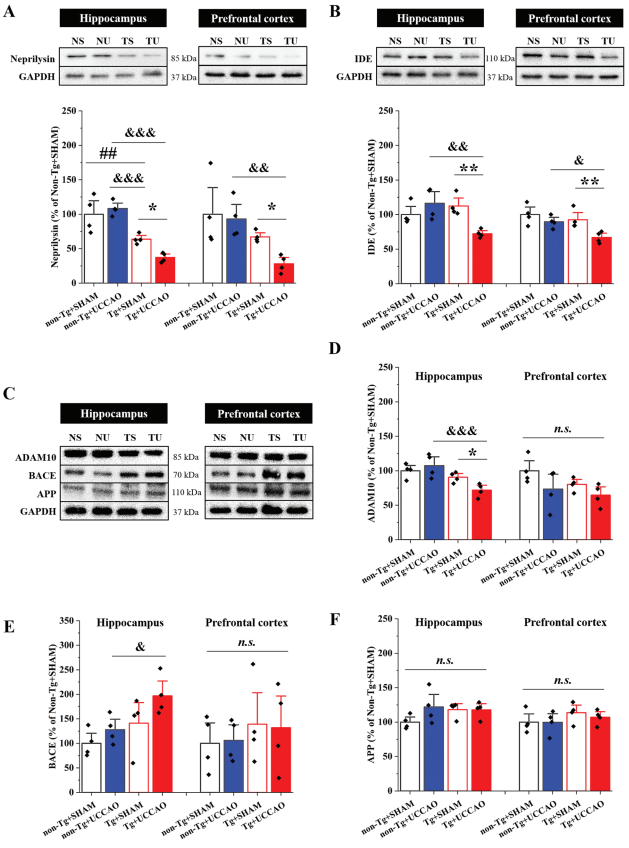

Figure 4. Expression level of proteins related Aβ production and clearance in the hippocampus and prefrontal cortex of 5XFAD mice with unilateral common carotid artery occlusion (UCCAO). (**A**) Western blotting for neprilysin and its quantification. (**B**) Western blotting for insulin-degrading enzyme (IDE) and its quantification. (**C**) Representative western blot images of proteins related Aβ production including ADAM10, β-site APP cleavage enzyme (BACE), and APP. Analyses were performed to quantify the expression of ADAM10 (**D**), BACE (**E**), and APP (**F**). Immunoreactive protein bands in each group were normalized to the internal control glyceraldehyde 3-phosphate dehydrogenase (GAPDH). $N = 4$ per group. Data are presented as the mean ± *SEM*. $^{\#\#}p < .01$ compared with non-Tg + SHAM group; $^{\&}p < .05$, $^{\&\&}p < .01$, and $^{\&\&\&}p < .001$ compared with non-Tg + UCCAO group; $^{*}p < .05$ and $^{**}p < .01$ compared with Tg + SHAM group. *n.s.* = nonsignificant.

Reduction of Neprilysin and IDE in the Hippocampus and PFC of 5XFAD + UCCAO Mice Is Correlated With the Loss of Reversal Memory

We conducted Pearson's correlation analysis to elucidate the potential role of the above-mentioned Aβ-related proteins in the reversal memory changes particularly observable in Tg + UCCAO. We analyzed the correlation between the number of new platform location entries in the reversal probe test of the water maze and the expression levels of each protein in the hippocampus and PFC, respectively (Supplementary Figure 7). In the hippocampus, there was a significant positive correlation between the number of new platform location entries and neprilysin ($R^2 = .4961$, $p = .002$), IDE ($R^2 = .4484$, $p = .005$), or ADAM10 levels ($R^2 = .3009$, $p = .028$). On the other hand, no significant correlation was detected between BACE or APP levels and the number of new platform location entries. In the PFC, the number of new platform location entries significantly correlated with the expression levels of neprilysin ($R^2 = .5078$, $p = .002$) or IDE ($R^2 = .4285$, $p = .006$), but not of ADAM10, BACE, or APP. These findings suggest a clear association between reversal memory deficits in 5XFAD mice after UCCAO, and decreased levels of enzymes related to Aβ clearance in the hippocampus and PFC.

Differences in Gene Expression in the Hippocampus and PFC Among Animal Models

To investigate the molecular differences among animal models, we measured gene expression levels in the hippocampus and PFC of each model. As shown in Figure 5A, we observed a clear difference in gene expression patterns between the 2 brain regions. However, within each region, similar gene expression patterns were observed (correlation coefficient > .4) among animal models. In particular, Tg and Tg + UCCAO models showed the highest correlation of gene expression in both the hippocampus and PFC. This pattern of similarity among samples was also observed when comparing the number of commonly expressed genes at the criterion of 1.5-fold ratio, as shown in Figure 5B. In addition, we observed that, compared to the other

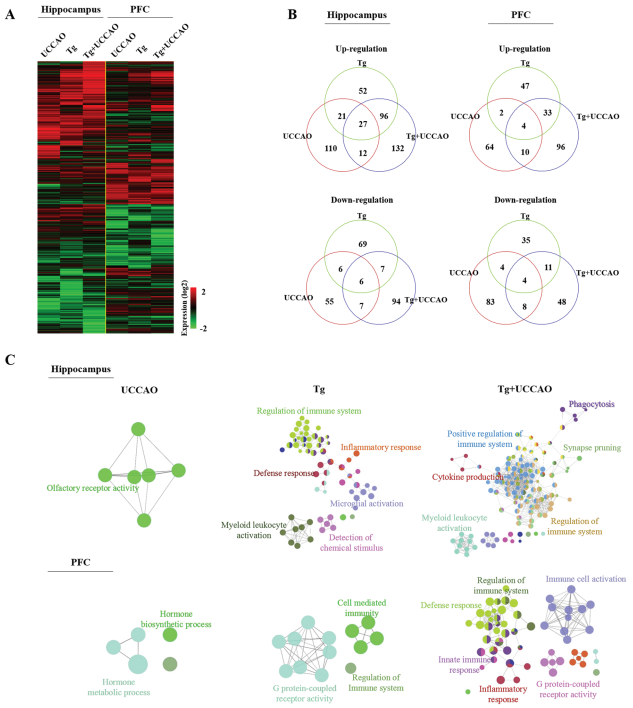

Figure 5. Gene expression patterns in the hippocampus and prefrontal cortex (PFC) of each model. (**A**) Differentially expressed genes (total: 3001 genes) showing an expression ratio >1.5 or <0.67 in at least one sample were hierarchically clustered. The columns represent individual samples and the rows individual genes. The red and green colors indicate up- and downregulation, respectively, as shown in the scale bar. (**B**) The number of differentially expressed genes was presented using a Venn diagram. (**C**) The functional association of differentially expressed genes was measured using ClueGO. The significantly enriched GO terms ($p < .01$) are represented as a network with names of representative functions in the hippocampus and PFC.

2 models, the largest number of genes differentially expressed in both the hippocampus and PFC were found in the Tg + UCCAO model. Thus, the biological functions associated with these differentially expressed genes were the most intricately interconnected, displayed as a huge network in both the hippocampus and PFC of the mixed models (Figure 5C). In particular, in this functional network, immune-related functions were significantly enriched ($p < .01$).

Pathway analysis also confirmed that immune-related pathways were activated in the Tg + UCCAO mouse model (Supplementary Figure 8A). In addition to these pathways, we also observed changes to diverse signaling pathways, including metabolism and signaling, in both the hippocampus and PFC. Consistent with the results on individual genes, a greater number of pathway activities (empirical p-value < .01) were altered in the Tg + UCCAO model than in the other 2 models (Supplementary Figure 8B). However, the pathway functions in the Tg + UCCAO model were significantly correlated with those in the Tg model ($p < .001$), supporting the molecular similarity between the 2 (Supplementary Figure 8C). In addition, significant similarities in pathway activities between the hippocampus and PFC were observed, especially in the Tg or Tg + UCCAO model ($p < .001$), as shown in Supplementary Figure 8D.

Discussion

Although AD and VaD share several key pathophysiology features in patients with dementia and overlap substantially in their comorbidity (34), the interaction between these 2 disorders has received relatively little attention. Herein, we sought to systematically investigate the effects of a reduction in cerebral perfusion on learning and memory in AD mice, and find their potential molecular basis. We found that cognitive flexibility was impaired in AD mice, and that CCH greatly exacerbated this impairment. We also observed a reduction in enzymes related to Aβ clearance in a CCH-induced AD mouse model, associated with increased Aβ plaque accumulation in the hippocampus and PFC. Interestingly, disruption of cognitive flexibility in 5XFAD mice following UCCAO was significantly correlated with decreased levels of Aβ-clearing-related enzymes, including neprilysin and IDE. This is the first study to report the interaction between CCH and AD in cognitive flexibility deficits associated with changes in Aβ metabolism.

People live in continuously changing environments, requiring us to learn and adapt to new lifestyles and ways of thinking. In this respect, cognitive flexibility, the ability to switch goal-directed adaptations in response to novel stimuli, is a crucial subdomain of brain function in humans (35). Several studies have reported impaired executive function related to cognitive flexibility in the early stages of AD (21,36). It has also been reported that low marks in the Trail Making Test, a criterion reflecting cognitive flexibility, is an indicator of high risk for cerebrovascular damage (37). These findings imply that patients with coexistent VaD and AD may struggle even more to maintain cognitive flexibility. The reversal version of the water maze task was used in the present study is known to explore behavioral flexibility in rodents (35,38). This task requires mice to learn the newly updated location of the platform, not the previously learned location. In the present study, we found indications of impaired reversal learning abilities in 5XFAD mice. Interestingly, after UCCAO, 5XFAD mice faced greater difficulties in learning the novel platform position than did the sham-exposed 5XFAD mice during reversal learning; the 5XFAD mice also failed to remember the updated platform location during the reversal probe test. Moreover, when we analyzed their searching strategies, UCCAO-exposed 5XFAD mice appeared to travel to previously learned quadrants, suggesting that CCH affected the ability of AD mice to adjust their behavior to learning new information and repressing previously learned information. These observations require future clinical studies to verify whether these alterations of cognitive flexibility also occur in patients with MD.

In the past decade, several approaches have aimed to investigate the effects of CCH on cognition in AD mice. Zhai et al. introduced bilateral common carotid artery stenosis in APP23 AD mice, resulting in exacerbated cognitive dysfunction in an 8-arm radial maze test (18). However, a severe impairment of motor performance was also observed in these Tg + CCH mice. Given that locomotor function could affect memory (39), this model cannot exclude the possibility that motor dysfunction influences synergistic memory impairment. In contrast, we investigated the cognition state of Tg + UCCAO mice, which show full motor abilities and has unimpaired visual function or anxiety levels, indicating its reliability for evaluating the basic cognitive function in MD. In addition, Pimentel-Coelho et al. (40) observed spatial learning impairments in the acquisition learning phase of the T-water maze task in APPswe/PS1 mice subjected to UCCAO, but not in the reversal learning phase, which is not in accordance with our data. One possible explanation for the difference between prior studies and ours is that the progress of the Aβ pathology varies depending on the mouse strain. The APPswe/PS1 mice used in Pimentel-Coelho et al.'s study are known to show a slow progression of

the AD phenotype relative to the 5XFAD mice used in the present study (41). This means that APPswe/PS1 mice can only be representative of the early phase of AD, which may not include a prolonged phase of AD. In addition, we conducted behavioral tasks 3 months after UCCAO, whereas Pimentel-Coelho et al. (40) conducted it 5 weeks thereafter. Previous studies reported that 2–3 months after CCH can be considered a chronic CCH stage, which highly reflects the pathophysiology in patients with dementia (17,42). Therefore, it is possible that CCH requires time to exert its effects on various types of memory, including reversal memory. In other words, it is important to select the appropriate experimental conditions, such as strain or time after CCH, for the detection of alterations in cognitive function.

To date, Aβ has been regarded as a major hallmark of AD and has been the driving force of Alzheimer's pathophysiology; thus, various approaches have aimed to targeting Aβ as therapeutic strategies for AD (43). In addition, increases in Aβ burden are found in individuals with CBF dysregulation (44). Based on prior studies, we examined Aβ plaque load in the mouse brain to investigate the potential role of Aβ pathology in memory reversal. Given that cognitive flexibility depends mostly on the interaction between the hippocampus and the PFC (35,38), we subsequently focused on the analysis of these 2 regions. Indeed, we observed significantly increased Aβ plaque deposition in the hippocampus and PFC of Tg + UCCAO mice compared to other groups. In line with the results of Aβ plaques, ELISA analysis demonstrated that UCCAO-exposed 5XFAD mice showed elevated Aβ40 and Aβ42 levels in the hippocampus and PFC. As abnormal Aβ generation is essential for its deposition, it can be inferred that in AD mice only, Aβ peptide overproduction due to CCH results in abnormal Aβ plaque growth.

Several studies have reported that Aβ deposition is further accelerated owing to an imbalance between Aβ clearance and generation (45,46). Aβ peptides are normally derived from APP, which is sequentially cleaved by BACE (amyloidogenic process). Otherwise, APP can be cleaved by ADAM10, which may not result in Aβ (non-amyloidogenic process). On the other hand, Aβ-degrading enzymes such as neprilysin and IDE process the clearance pathway for Aβ. Interestingly, we found a significant reduction in the expression levels of neprilysin and IDE, with a slight alteration in the levels of ADAM10 and BACE, in the hippocampus and PFC of UCCAO-exposed 5XFAD mice. Considering previous reports on decreased β clearance–related enzymes due to hypoxia/ischemia or Aβ overexpression (47,48), we can speculate that CCH could additively or synergistically contribute to the imbalance between Aβ production and removal in AD. It should be noted that there was a strong positive correlation between the expression levels of enzymes related to Aβ clearance and the measure of cognitive flexibility in the water maze task. Although we cannot infer causality from this, this change in Aβ clearance enzyme levels might be one molecular evidence linking CCH with AD. In addition, although this study did not investigate CCH, there is recent evidence suggesting that impairment of Aβ clearance may be occurring in hypoperfused brains due to atherosclerosis, which is associated with reduction in Aβ solute transport in the perivascular space (49). Based on an earlier report showing that vascular–perivascular pathways play a key role in Aβ clearance (50), the effect of CCH on Aβ solute exchange via perivascular pathways in AD brain should be investigated in the future.

While the relationship between CCH and AD requires additional research, experimental data from other studies suggest that AD pathology and vascular dysfunction interact additionally/synergistically to promote brain damage. Cerebrovascular insufficiency enhances Aβ production and accumulation, which in turn induces vascular inflammation and oxidative stress (49,51). This inextricable link between the 2 factors was further developed into the 2-hit hypothesis of AD (13,14,52). Specifically, Aβ-independent mechanism (hit 1), which states that CBF reductions and dysregulation may cause damage to the machinery of Aβ clearance, is followed by Aβ-dependent mechanism (hit 2), or the neurotoxic effects of Aβ-induced vascular dysfunction. In support of this hypothesis, our results showed that Aβ accumulation in 5XFAD mice was significantly increased under UCCAO-induced CCH condition; moreover, there was a decrease in the level of Aβ clearance–related protein, which reflects "hit 1" of the hypothesis. Future studies are warranted to further investigate "hit 2" of the hypothesis.

The aforementioned results indicate that CCH could affect the additional decline in levels of enzymes related to Aβ clearance in AD mice, yet how CCH modulates relevant mechanisms remains elusive. Prior studies have provided some possible explanations. Ashok et al. reported that increased heparin-binding EGF-like growth factor (HB-EGF) induced its transcription factor, resulting in the disintegration of the blood–brain barrier, causing an impairment of Aβ clearance under CCH conditions (53). Thus, it would be valuable to investigate whether there is any crosstalk between HB-EGF and Aβ pathology in a mixed mouse model of CCH and AD. Epigenetic alterations in gene expression of Aβ clearance proteins may be another possible explanation. It has been reported that hypoxia reduces neprilysin gene expression by facilitating histone modifications in the gene promoter, which can be reversed by inhibition of histone deacetylase (HDAC) (54). Recently, treatment with HDAC inhibitors has shown promise in preclinical trials with AD as well as ischemic stroke (55,56). Considering these reports, future research on posttranslational histone modification in MD mouse models could be worthwhile.

Lastly, we performed microarray analyses and compared gene expression in the hippocampus and PFC among the experimental groups. We also applied gene set–based approaches to determine whether there might be changes in the functional association of genes. Importantly, we found that pathway activities, including individual genes, were dramatically different in UCCAO-exposed 5XFAD mice than in the other mice. In other words, exposure of Tg mice to UCCAO can cause additive and/or synergistic regulation of gene transcription in the brain. Considering all the present data, including cognitive and histological results, the microarray analyses raised the possibility of an interaction between CCH and AD. Future studies targeting their relationship using major responsive genes in diverse MD mouse models could be the optimal method for elucidating the precise mechanisms of MD.

Our study had several limitations that need to be discussed. First, assessment of cognitive flexibility is required to demonstrate a causal link when enzymes related to Aβ clearance are genetically or surgically upregulated in a MD mouse model. Second, a network analysis of functional connectivity using resting-state functional magnetic resonance imaging in MD mouse models would be useful to understand the spatiotemporal dynamics during the cognitive process in reversal learning. Lastly, while the present research focused on the analysis of Aβ pathology, it will be interesting to study the relationship between cognitive flexibility and tauopathy, another main pathological hallmark in AD (57).

In conclusion, our study demonstrated that CCH could synergistically interact with Aβ pathology in 5XFAD Tg mice, and that it was highly correlated with reversal learning deficits. This alteration in cognitive behavior provides a platform for studying the effect of

CCH on cognitive flexibility in AD. Future studies on the neurobiological mechanisms of impaired cognitive flexibility in MD are needed to develop therapeutic candidates for further clinical trials.

Supplementary Material

Supplementary data are available at *The Journals of Gerontology, Series A: Biological Sciences and Medical Sciences* online.

Funding

This work was supported by grants from the National Research Council of Science and Technology (NST) by the Korean government (MSIP) (CRC-15-04-KIST, KSN1621850, and NSN1522380).

Conflict of Interest

None declared.

Author Contributions

M.-S.K.: study design and conceptualization; methodology; acquisition, analysis, and interpretation of data; and writing of the draft. J.B.: methodology and analysis of data. B.-Y.K.: methodology, analysis of data, and writing of the draft. W.K.J.: funding acquisition and project administration.

References

1. Cummings J, Lee G, Ritter A, Sabbagh M, Zhong K. Alzheimer's disease drug development pipeline: 2019. *Alzheimers Dement (NY)*. 2019;5:272–293. doi:10.1016/j.trci.2019.05.008
2. Kazui H, Yoshiyama K, Kanemoto H, et al. Differences of behavioral and psychological symptoms of dementia in disease severity in four major dementias. *PLoS ONE*. 2016;11:e0161092. doi:10.1371/journal.pone.0161092
3. Androsova L, Mikhaylova N, Zozulya S, Dupin A, Klyushnik T. A comparative study of innate immunity markers in Alzheimer's disease, mixed dementia and vascular dementia. *Int J Clin Neurosci Ment Health*. 2016;3(suppl. 1):03. doi:10.21035/ijcnmh.2016.3(Suppl.1).S03
4. Attems J, Jellinger KA. The overlap between vascular disease and Alzheimer's disease—lessons from pathology. *BMC Med*. 2014;12:206. doi:10.1186/s12916-014-0206-2
5. Love S, Miners JS. Cerebrovascular disease in ageing and Alzheimer's disease. *Acta Neuropathol*. 2016;131:645–658. doi:10.1007/s00401-015-1522-0
6. Miki K, Ishibashi S, Sun L, et al. Intensity of chronic cerebral hypoperfusion determines white/gray matter injury and cognitive/motor dysfunction in mice. *J Neurosci Res*. 2009;87:1270–1281. doi:10.1002/jnr.21925
7. Huang LA, Li W, Wei D, Liang J, Xie X, Song K. Comprehensive evaluation of white matter damage and neuron death and whole-transcriptome analysis of rats with chronic cerebral hypoperfusion. *Front Cell Neurosci*. 2019;13:310. doi:10.3389/fncel.2019.00310
8. Farkas E, Luiten PG, Bari F. Permanent, bilateral common carotid artery occlusion in the rat: a model for chronic cerebral hypoperfusion-related neurodegenerative diseases. *Brain Res Rev*. 2007;54:162–180. doi:10.1016/j.brainresrev.2007.01.003
9. Vinciguerra L, Lanza G, Puglisi V, et al. Update on the neurobiology of vascular cognitive impairment: from lab to clinic. *Int J Mol Sci*. 2020;21:2977. doi:10.3390/ijms21082977
10. Toyama K, Koibuchi N, Uekawa K, et al. Apoptosis signal–regulating kinase 1 is a novel target molecule for cognitive impairment induced by chronic cerebral hypoperfusion. *Arterioscl Throm Vas*. 2014;34:616–625. doi:10.1161/ATVBAHA.113.302440
11. Duncombe J, Kitamura A, Hase Y, Ihara M, Kalaria RN, Horsburgh K. Chronic cerebral hypoperfusion: a key mechanism leading to vascular cognitive impairment and dementia. Closing the translational gap between rodent models and human vascular cognitive impairment and dementia. *Clin Sci (Lond)*. 2017;131:2451–2468. doi:10.1042/CS20160727
12. Zou W, Song Y, Li Y, Du Y, Zhang X, Fu J. The role of autophagy in the correlation between neuron damage and cognitive impairment in rat chronic cerebral hypoperfusion. *Mol Neurobiol*. 2018;55:776–791. doi:10.1007/s12035-016-0351-z
13. Wierenga CE, Hays CC, Zlatar ZZ. Cerebral blood flow measured by arterial spin labeling MRI as a preclinical marker of Alzheimer's disease. *J Alzheimers Dis*. 2014;42(suppl. 4):S411–S419. doi:10.3233/JAD-141467
14. Solis E, Hascup KN, Hascup ER. Alzheimer's disease: the link between amyloid-β and neurovascular dysfunction. *J Alzheimers Dis*. 2020;76:1179–1198. doi:10.3233/JAD-200473
15. Takeda S, Rakugi H, Morishita R. Roles of vascular risk factors in the pathogenesis of dementia. *Hypertens Res*. 2020;43:162–167. doi:10.1038/s41440-019-0357-9
16. Pluta R, Ułamek-Kozioł M, Januszewski S, Czuczwar SJ. Shared genomic and proteomic contribution of amyloid and tau protein characteristic of Alzheimer's disease to brain ischemia. *Int J Mol Sci*. 2020;21:3186. doi:10.3390/ijms21093186
17. Yamada M, Ihara M, Okamoto Y, et al. The influence of chronic cerebral hypoperfusion on cognitive function and amyloid β metabolism in APP overexpressing mice. *PLoS ONE*. 2011;6:e16567. doi:10.1371/journal.pone.0016567
18. Zhai Y, Yamashita T, Nakano Y, et al. Chronic cerebral hypoperfusion accelerates Alzheimer's disease pathology with cerebrovascular remodeling in a novel mouse model. *J Alzheimers Dis*. 2016;53:893–905. doi:10.3233/JAD-160345
19. Shang J, Yamashita T, Zhai Y, et al. Acceleration of NLRP3 inflammasome by chronic cerebral hypoperfusion in Alzheimer's disease model mouse. *Neurosci Res*. 2019;143:61–70. doi:10.1016/j.neures.2018.06.002
20. Lee JS, Im DS, An Y-S, Hong JM, Gwag BJ, Joo IS. Chronic cerebral hypoperfusion in a mouse model of Alzheimer's disease: an additional contributing factor of cognitive impairment. *Neurosci Lett*. 2011;489:84–88. doi:10.1016/j.neulet.2010.11.071
21. Albert MS. Cognitive and neurobiologic markers of early Alzheimer disease. *Proc Natl Acad Sci USA*. 1996;93:13547–13551. doi:10.1073/pnas.93.24.13547
22. Sadleir KR, Popovic J, Vassar R. ER stress is not elevated in the 5XFAD mouse model of Alzheimer's disease. *J Biol Chem*. 2018;293:18434–18443. doi:10.1074/jbc.RA118.005769
23. Kim M-S, Bang J, Jeon WK. The involvement of canonical Wnt signaling in memory impairment induced by chronic cerebral hypoperfusion in mice. *Transl Stroke Res*. 2020;11:734–746. doi:10.1007/s12975-019-00748-1
24. Sun K, Sun Y, Li H, et al. Anti-ageing effect of *Physalis alkekengi* ethyl acetate layer on a D-galactose-induced mouse model through the reduction of cellular senescence and oxidative stress. *Int J Mol Sci*. 2020;21:1836. doi:10.3390/ijms21051836
25. Park M, Kim CH, Jo S, et al. Chronic stress alters spatial representation and bursting patterns of place cells in behaving mice. *Sci Rep*. 2015;5:16235. doi:10.1038/srep16235
26. Latif-Hernandez A, Shah D, Ahmed T, et al. Quinolinic acid injection in mouse medial prefrontal cortex affects reversal learning abilities, cortical connectivity and hippocampal synaptic plasticity. *Sci Rep*. 2016;6:36489. doi:10.1038/srep36489
27. Lo AC, De Maeyer JH, Vermaercke B, Callaerts-Vegh Z, Schuurkes JA, D'Hooge R. SSP-002392, a new 5-HT4 receptor agonist, dose-dependently reverses scopolamine-induced learning and memory impairments in C57Bl/6 mice. *Neuropharmacology*. 2014;85:178–189. doi:10.1016/j.neuropharm.2014.05.013
28. Kim MS, Choi BR, Lee YW, et al. Chronic cerebral hypoperfusion induces alterations of matrix metalloproteinase-9 and angiopoietin-2 levels in the rat hippocampus. *Exp Neurobiol*. 2018;27:299–308. doi:10.5607/en.2018.27.4.299
29. Sagare AP, Bell RD, Zhao Z, et al. Pericyte loss influences Alzheimer-like neurodegeneration in mice. *Nat Commun*. 2013;4:2932. doi:10.1038/ncomms3932

30. Bang J, Kim M-S, Jeon WK. Mumefural ameliorates cognitive impairment in chronic cerebral hypoperfusion via regulating the septohippocampal cholinergic system and neuroinflammation. *Nutrients*. 2019;11:2755. doi:10.3390/nu11112755
31. Kraeuter AK, Guest PC, Sarnyai Z. The Y-maze for assessment of spatial working and reference memory in mice. *Methods Mol Biol*. 2019;1916:105–111. doi:10.1007/978-1-4939-8994-2_10
32. Chudasama Y, Doobay VM, Liu Y. Hippocampal-prefrontal cortical circuit mediates inhibitory response control in the rat. *J Neurosci*. 2012;32:10915–10924. doi:10.1523/JNEUROSCI.1463-12.2012
33. Musardo S, Marcello E. Synaptic dysfunction in Alzheimer's disease: from the role of amyloid β-peptide to the α-secretase ADAM10. *Eur J Pharmacol*. 2017;817:30–37. doi:10.1016/j.ejphar.2017.06.018
34. de la Torre J. The vascular hypothesis of Alzheimer's disease: a key to preclinical prediction of dementia using neuroimaging. *J Alzheimers Dis*. 2018;63:35–52. doi:10.3233/JAD-180004
35. Anacker C, Hen R. Adult hippocampal neurogenesis and cognitive flexibility—linking memory and mood. *Nat Rev Neurosci*. 2017;18:335–346. doi:10.1038/nrn.2017.45
36. Mueller SM, Arias MG, Mejuto Vázquez G, Schiebener J, Brand M, Wegmann E. Decision support in patients with mild Alzheimer's disease. *J Clin Exp Neuropsychol*. 2019;41:484–496. doi:10.1080/13803395.2019.1585517
37. Wiberg B, Lind L, Kilander L, Zethelius B, Sundelöf JE, Sundström J. Cognitive function and risk of stroke in elderly men. *Neurology*. 2010;74:379–385. doi:10.1212/WNL.0b013e3181ccc516
38. Shah D, Latif-Hernandez A, De Strooper B, et al. Spatial reversal learning defect coincides with hypersynchronous telencephalic BOLD functional connectivity in APPNL-F/NL-F knock-in mice. *Sci Rep*. 2018;8:6264. doi:10.1038/s41598-018-24657-9
39. Lindgren HS, Dunnett SB. Cognitive dysfunction and depression in Parkinson's disease: what can be learned from rodent models? *Eur J Neurosci*. 2012;35:1894–1907. doi:10.1111/j.1460-9568.2012.08162.x
40. Pimentel-Coelho PM, Michaud JP, Rivest S. Effects of mild chronic cerebral hypoperfusion and early amyloid pathology on spatial learning and the cellular innate immune response in mice. *Neurobiol Aging*. 2013;34:679–693. doi:10.1016/j.neurobiolaging.2012.06.025
41. Kosel F, Torres Munoz P, Yang JR, Wong AA, Franklin TB. Age-related changes in social behaviours in the 5xFAD mouse model of Alzheimer's disease. *Behav Brain Res*. 2019;362:160–172. doi:10.1016/j.bbr.2019.01.029
42. Zhang X, Huang X, Fang C, et al. miR-124 regulates the expression of BACE1 in the hippocampus under chronic cerebral hypoperfusion. *Mol Neurobiol*. 2017;54:2498–2506. doi:10.1007/s12035-016-9845-y
43. Madav Y, Wairkar S, Prabhakar B. Recent therapeutic strategies targeting beta amyloid and tauopathies in Alzheimer's disease. *Brain Res Bull*. 2019;146:171–184. doi:10.1016/j.brainresbull.2019.01.004
44. Sojkova J, Beason-Held L, Zhou Y, et al. Longitudinal cerebral blood flow and amyloid deposition: an emerging pattern? *J Nucl Med*. 2008;49:1465–1471. doi:10.2967/jnumed.108.051946
45. Cho GM, Lee SY, Park JH, et al. Photobiomodulation using a low-level light-emitting diode improves cognitive dysfunction in the 5XFAD mouse model of Alzheimer's disease. *J Gerontol A Biol Sci Med Sci*. 2020;75:631–639. doi:10.1093/gerona/gly240
46. Zhou L, Liu J, Dong D, Wei C, Wang R. Dynamic alteration of neprilysin and endothelin-converting enzyme in age-dependent APPswe/PS1dE9 mouse model of Alzheimer's disease. *Am J Transl Res*. 2017;9:184–196.
47. Nalivaevaa NN, Fisk L, Kochkina EG, et al. Effect of hypoxia/ischemia and hypoxic preconditioning/reperfusion on expression of some amyloid-degrading enzymes. *Ann NY Acad Sci*. 2004;1035:21–33. doi:10.1196/annals.1332.002
48. Hüttenrauch M, Baches S, Gerth J, Bayer TA, Weggen S, Wirths O. Neprilysin deficiency alters the neuropathological and behavioral phenotype in the 5XFAD mouse model of Alzheimer's disease. *J Alzheimers Dis*. 2015;44:1291–1302. doi:10.3233/JAD-142463
49. Gupta A, Iadecola C. Impaired Aβ clearance: a potential link between atherosclerosis and Alzheimer's disease. *Front Aging Neurosci*. 2015;7:115. doi:10.3389/fnagi.2015.00115
50. Roberts KF, Elbert DL, Kasten TP, et al. Amyloid-β efflux from the central nervous system into the plasma. *Ann Neurol*. 2014;76:837–844. doi:10.1002/ana.24270
51. Cortes-Canteli M, Iadecola C. Alzheimer's disease and vascular aging: JACC focus seminar. *J Am Coll Cardiol*. 2020;75:942–951. doi:10.1016/j.jacc.2019.10.062
52. Kisler K, Nelson AR, Montagne A, Zlokovic BV. Cerebral blood flow regulation and neurovascular dysfunction in Alzheimer disease. *Nat Rev Neurosci*. 2017;18:419–434. doi:10.1038/nrn.2017.48
53. Ashok A, Rai NK, Raza W, Pandey R, Bandyopadhyay S. Chronic cerebral hypoperfusion-induced impairment of Aβ clearance requires HB-EGF-dependent sequential activation of HIF1α and MMP9. *Neurobiol Dis*. 2016;95:179–193. doi:10.1016/j.nbd.2016.07.013
54. Wang Z, Yang D, Zhang X, et al. Hypoxia-induced down-regulation of neprilysin by histone modification in mouse primary cortical and hippocampal neurons. *PLoS ONE*. 2011;6:e19229. doi:10.1371/journal.pone.0019229
55. Yang SS, Zhang R, Wang G, Zhang YF. The development prospection of HDAC inhibitors as a potential therapeutic direction in Alzheimer's disease. *Transl Neurodegener*. 2017;6:19. doi:10.1186/s40035-017-0089-1
56. Matheson R, Chida K, Lu H, et al. Neuroprotective effects of selective inhibition of histone deacetylase 3 in experimental stroke. *Transl Stroke Res*. 2020;11:1052–1063. doi:10.1007/s12975-020-00783-3
57. Ittner A, Ittner LM. Dendritic tau in Alzheimer's disease. *Neuron*. 2018;99:13–27. doi:10.1016/j.neuron.2018.06.003